Shape of prismatic dislocation loops in anisotropic crystals

Steven P. Fitzgerald*

EURATOM/UKAEA Fusion Association,

Culham Science Centre, Abingdon, UK, OX14 3DB

Zhongwen Yao

Department of Materials, University of Oxford,

Parks Road, Oxford, UK, OX1 3PH

Abstract

Prismatic dislocation loops are the primary manifestation of radiation damage in crystals, and contribute to the phenomenon of radiation embrittlement. This undesirable effect, most serious for materials used in high-dose environments such as next-generation fission and future fusion reactors, results from the strong interaction between gliding dislocations, the carriers of plasticity, with the population of radiation-induced prismatic loops. Ferritic-martensitic steels, the most promising candidate materials for future high-dose applications, are based on iron, and are known to become highly elastically-anisotropic at the high temperatures (>500 ℃) at which they must operate. In this paper, we develop a novel modelling approach based on anisotropic elasticity theory to predict the shapes of prismatic loops in anisotropic crystals, paying particular attention to the technologically-important case of α-iron. The results are compared with transmission electron microscope observations of the damage structure sustained by ultra-high-purity iron irradiated to a dose of ~ 2 displacements per atom.

PACS numbers: 61.72.Bb,61.72.Ff,61.82,Bg

*Electronic address: steve.fitzgerald@ukaea.org.uk

Introduction– Prismatic dislocation loops form by the aggregation of single self-interstitial atomic (SIA) or vacancy defects. They can grow or shrink only by the absorption of further defects, and are free to move conservatively only along the edges of the prism defined by the continuation of their perimeter along the crystallographic direction of their Burgers' vector. At nucleation they have pure edge character, but can in some circumstances tilt with respect to the prism axis, and acquire a screw component [1]. Prismatic loops act as obstacles to the motion of gliding dislocations, and are a significant cause of embrittlement in irradiated metals, where the high density of Frenkel pairs of single-atom defects created by the incident particles leads to a large population of the loops. In highly-irradiated samples, a "sea" of smaller defects is also observed [2], which also contribute to the embrittlement, acting in a similar manner.

In an isotropic medium, since the direction of its dislocation line is everywhere orthogonal to its Burgers' vector, any prismatic loop is circular. This is at odds with observations in the microscope [3, 4] and atomistic simulations [5, 6] however, where hexagonal or square loops are often observed and modelled. Moreover, a loop's shape defines the character of its sides, which control the interaction with glide dislocations and hence the effects on mechanical properties. Understanding the structure and behaviour of these defects is essential if we wish to link the microscopic properties of radiation damage with the mechanical behaviour of radiation-resistant materials for use in future next-generation fission and fusion reactors. The most promising candidate materials for these vital applications are reduced-activation-ferritic-martenstic steels based on Fe, whose significant high-temperature elastic anisotropy is well known [6–8].

In this paper we use anisotropic linear elasticity theory to predict, via a variational approach, the shapes of prismatic dislocation loops for arbitrary elastic anisotropy. We extend the original approach developed by deWit and Koehler [9], where for sufficient anisotropy puzzling cusped, self-crossing dislocation configurations were predicted. Here we show how such unphysical behaviour can be avoided by the appropriate mathematical treatment of corners on the loops. Dislocation lines with sharp corners have been observed in the microscope [10, 11], and can be qualitatively explained [6, 12] by the direction-dependence of the elastic energy of dislocations in an anisotropic crystal: if a segment is pinned in an energetically-unfavourable direction, it will be unstable to the formation of a bent or zigzagged configuration, if the resulting line directions save sufficient energy to compensate

for the increase in overall segment length. This behaviour is signalled by the dislocation's line tension in the original direction being negative, corresponding to a concave region in the plot of the line energy vs. angle [13, 14], a Wulff construction [15]. Originally devised to model crystal growth, the Wulff construction applies to any process governed by the anisotropic orientation-dependence of the energy of a boundary, see *e.g.* [16] and references therein.

α-iron is known to become highly anisotropic at high temperatures [6–8], and applying our results allows direct comparison with our transmission electron microscope (TEM) observations,and Molecular Dynamics (MD) computer simulations. The approach described here also sheds light on the general issue of dislocation instability, in particular the prediction of configurations containing sharp corners.

Governing equations– The local part of the elastic energy of a dislocation line element depends only on the element's direction, Burgers' vector, and the elastic moduli of the crystal [17]. We note that the full expression for the loop's energy involves non-local terms [18] and the non-elastic core energy [6], and neglecting these terms is a serious simplification. However, the results will be valid for loops sufficiently large (a few tens of nanometres) that the dominant contribution is the local elastic term.

We wish to minimize the line energy of the loop whilst keeping its area constant, corresponding to a fixed number of SIAs or vacancies. The area per SIA/vacancy depends on the loop's orientation, but for the purposes of determining the equilibrium loop shape this can be absorbed into the Lagrange multiplier introduced below.

The energy of a loop C is given in this approximation by

$$\text{self energy} = \ln\left(\frac{R}{\epsilon}\right)\oint_C \mathcal{E}\,\mathrm{d}s = \ln\left(\frac{R}{\epsilon}\right)\int_{\lambda_1}^{\lambda_2}\mathcal{E}\,\frac{\mathrm{d}s}{\mathrm{d}\lambda}\,\mathrm{d}\lambda, \tag{1}$$

where $\mathcal{E}$ is the direction-dependent prelogarithmic energy factor [19]. R and ϵ are outer and inner cutoffs respectively and λ is a monotonically-increasing parameter around the curve, introduced to allow the perimeter to vary (we can neglect the logarithmic part as it will affect only the overall scale of the curve and not the shape). The resulting shape will be the outcome of the competition between the total length and the orientations of the sides. Plots of $\mathcal{E}$ vs. orientation in the loop plane are given in the upper pane of Fig.1 for $\boldsymbol{b} = [100]$ in Fe at 900 ℃ ($C_{12} = 122.2, C_{44} = 99.0, C' = 13.3$ GPa [20]). The energy per unit length is lower *for all orientations* of a prismatic loop, compared to the isotropic approximation,

where the two shear moduli are replaced by their mean. In the isotropic case there is no angular variation, since all edge orientations are equivalent. Thus there is no competition between total length and orientation, resulting in a circular loop.

Parameterizing the curve C with the coordinates $(x(\lambda), y(\lambda))$ in the loop's plane, its shape will be given by the (x, y) that minimize the integral

$$\int_{\lambda_1}^{\lambda_2} \left\{ \mathcal{E}\left(\dot{x}, \dot{y}\right) \sqrt{\dot{x}^2 + \dot{y}^2} + \frac{\mu}{2} \left(x\dot{y} - y\dot{x}\right) \right\} \mathrm{d}\lambda, \tag{2}$$

where overdots indicate differentiation with respect to λ, and μ is a Lagrange multiplier introduced to enforce the area constraint of the second term. Introducing the tangent angle ψ, $\tan\psi = \mathrm{d}y/\mathrm{d}x = \dot{y}/\dot{x}$, the coupled Euler-Lagrange equations read

$$\begin{aligned} 0 &= \frac{\mathrm{d}}{\mathrm{d}\lambda} \left\{ \mathcal{E} \sin\psi + \cos\psi \frac{\mathrm{d}\mathcal{E}}{\mathrm{d}\psi} + \mu x \right\}; \\ 0 &= \frac{\mathrm{d}}{\mathrm{d}\lambda} \left\{ \mathcal{E} \cos\psi - \sin\psi \frac{\mathrm{d}\mathcal{E}}{\mathrm{d}\psi} - \mu y \right\}, \end{aligned} \tag{3}$$

i.e. the quantities in braces are conserved around the curve. Differentiating these with respect to ψ and transforming to in-plane intrinsic coordinates (s, ψ) leads to the single equation

$$\mu \frac{\mathrm{d}s}{\mathrm{d}\psi} = \mathcal{E}(\psi) + \mathcal{E}(\psi)'' = \rho(\psi), \tag{4}$$

in agreement with Ref.[9]. The prime denotes differentiation with respect to ψ, and we have introduced the curve length s. μ can be set equal to one as it only affects the overall scale of the curve, and $\mathrm{d}s/\mathrm{d}\psi$ is the local radius of curvature ρ, set by the line tension $\mathcal{E}(\psi) + \mathcal{E}(\psi)''$. In an isotropic crystal this is always positive, leading to a convex curve, but when the crystal is anisotropic, it can be positive, negative or zero, corresponding to local convexity, concavity and cusp respectively (Fig.1 (bottom pane) shows the line tension vs. glide plane angle for a $\boldsymbol{b} = [100]$ loop in α-Fe at 900 ℃). If $\rho(\psi)$ contains zeros, then the curve $s(\psi)$ cannot simply be plotted "from $\psi = 0$ to 2π", as ψ will not increase monotonically around the curve; attempting to do this leads to the unphysical self-crossing curves predicted in Ref.[9].

Broken extremals and the Weierstrass-Erdmann conditions– To plot the loop according to (4) it must be divided into sections where ρ is away from zero. This will supply segments of curve which satisfy the variational condition, but it is not immediately clear how to link them into a physical solution. Solutions with discontinuities in the derivatives (*i.e.*

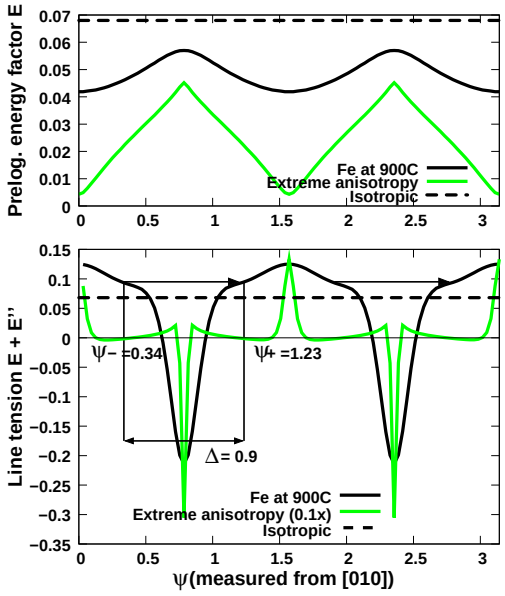

FIG. 1: (Colour online) Prelogarithmic energy factor (top) and line tension (bottom) vs. angle from [010] direction; $\boldsymbol{b} = [100]$; only $\psi = 0$ to π shown. Black solid line: Fe at 900 ℃ ; green (lighter solid line): extreme anisotropy with $C_{44}/C' \sim 700$ (0.1× scale in lower plot); black dashed line: the isotropic approximation.

loops with corners) must satisfy the Weierstrass-Erdmann (WE) conditions [21], which for a variational integrand F impose the following continuity requirements at each corner:

$$\left[\frac{\partial F}{\partial y'}\right]_-^+ = 0; \qquad \left[F - y'\frac{\partial F}{\partial y'}\right]_-^+ = 0. \tag{5}$$

These correspond precisely to the conservation of the quantities in braces in (3). At a corner, ψ will jump by an *a priori* unknown amount $\Delta \equiv \psi^+ - \psi^-$, and the WE conditions become

$$\begin{aligned} \mathcal{E}(\psi^- + \Delta)' &= \mathcal{E}(\psi^-)'\cos\Delta - \mathcal{E}(\psi^-)\sin\Delta; \\ \mathcal{E}(\psi^- + \Delta) &= \mathcal{E}(\psi^-)\cos\Delta + \mathcal{E}(\psi^-)'\sin\Delta. \end{aligned} \tag{6}$$

These equations can be simplified by exploiting the symmetry of the problem. The plot of $\mathcal{E}$ vs. ψ for the $\boldsymbol{b} = [100]$ energy curve in Fig.1 (top pane) shows that the minimum energy orientations occur at $\psi = 0, \pi/2, \pi, 3\pi/2$, corresponding to the cubic axes, and the maxima between are at $\pi/4, 3\pi/4, 5\pi/4, 7\pi/4$. It is reasonable to assume that the sides of the loop are oriented at angles near the minima, and the corners allow the omission of the angles near the maxima. To this end, we look for a solution of (6) such that $\psi^- = \pi/4 - \Delta/2$; $\psi^+ =$

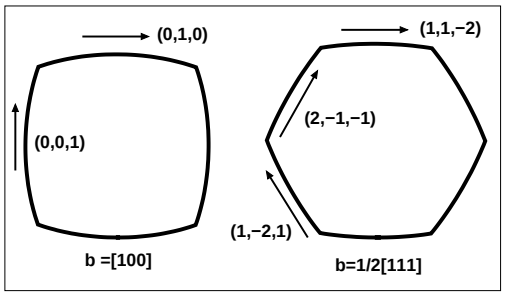

FIG. 2: Predicted prismatic loop shapes for highly-anisotropic 900 ℃ Fe (arbitrary scale). The loop sides align themselves along the lowest-energy directions, {001}-type for $\boldsymbol{b} = [100]$ (left), and $\{11\bar{2}\}$-type for $\boldsymbol{b} = 1/2[111]$ (right).

$\pi/4 + \Delta/2$. Using the even/odd symmetry of the functions $\mathcal{E}$ and $\mathcal{E}'$ about the extrema, the WE conditions reduce to

$$\tan\frac{\Delta}{2} = -\frac{\mathcal{E}\left(\frac{\pi}{4}+\frac{\Delta}{2}\right)'}{\mathcal{E}\left(\frac{\pi}{4}+\frac{\Delta}{2}\right)}, \tag{7}$$

which can be solved graphically for Δ and hence $\psi^{\pm}$. In the isotropic limit, $\mathcal{E}' = 0$, so (7) gives $\Delta = 0$, and no corners. The example of Fe at 900 ℃ leads to $\psi^{-} = 0.337$; $\psi^{+} = 1.234$ rad., so the highest-energy orientations are avoided (along with the region of negative curvature). The other orientations follow from the fourfold symmetry. In Fig.1, the jumps are indicated by the horizontal arrows. The shape of the loop is obtained by integrating Eq.(4), omitting the ranges of ψ prescribed by the WE conditions. Only the ranges between a ψ^{+} and the subsequent ψ^{-} are realized, leading to sides which appear almost straight (Fig.2 left). As the extreme case illustrates (Fig.1), smaller and smaller ranges of ψ are included as the anisotropy increases, leading in the limit $C' \to 0$ to completely straight sides aligned along the minimum energy directions. In this limit, the energy associated with those directions reaches zero, and hence no competition between orientation and curve length remains. The same procedure can be repeated for $\boldsymbol{b} = 1/2[111]$ with $\pi/4 \to \pi/6$ for the sixfold symmetry of the $1/2[111]$ energy curve, where $\psi^{-,+} = 0.16, 0.89 + n\pi/6$. This leads to the hexagonal shape shown in Fig.2 right, in excellent agreement with the observations of β-brass in Ref.[3], which exhibits similar anisotropy to high temperature Fe.

Mid-temperature predictions and TEM observations– We carried out *in situ* irradiation of thin foils of ultra-high-purity Fe (UHP-Fe) with 150 keV heavy ions (Fe^{+}), to a dose of 2 displacements per atom (dpa), at 400 and 500 ℃ , resulting in a large population of

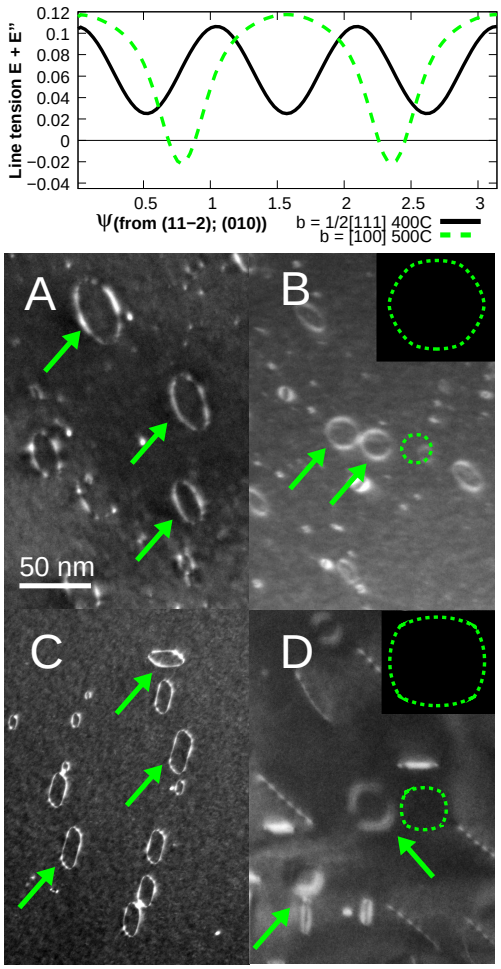

FIG. 3: Top: line tension for $\boldsymbol{b} = 1/2[111]$ and [100] prismatic loop orientations in Fe at 400 and 500 ℃ respectively. Micrographs showing radiation damage in ultra-high-purity Fe irradiated to 2 dpa at 400 ℃ (centre) and 500 ℃ (bottom). Predicted shapes are shown in the micrograph insets, including scaled versions for direct comparison with observed loops, see text.

prismatic dislocation loops 10-50 nm in diameter. At 400 ℃ , most of the large loops are of $1/2\langle 111\rangle$ interstitial type, but when the temperature is increased to 500 ℃ , only $\langle 100\rangle$ loops are observed. This is in agreement with the calculations of Ref.[6], which predict precisely this crossover behaviour when the relative stability of the two orientations is reversed as the elastic anisotropy increases with temperature. Also confirmed are the shape predictions made above. The loops in the sample irradiated at 400 ℃ (Fig.3A and B) are smooth-sided and almost circular (the loops in Fig.3A appear elliptical because of the viewing angle; they are in fact circular as in Fig.3B). The samples irradiated at 500 ℃ , however (Fig.3C and D), show straight-sided squared-off $\langle 100\rangle$ loops with corners, consistent with the line tension

plots of Fig.3 (top) (the rhomboidal shapes in Fig.3 C *c.f.* D are again due to the viewing angle. This is also responsible for the fact that two opposite corners of the central square loop in Fig.3 D are invisible and only come into view as the sample is tilted with respect to the electron beam).

Fig.3 (top) shows the variation of line tension with angle for the two types of prismatic loop under consideration. At 400 ℃ , the elastic anisotropy is insufficient for the $\boldsymbol{b} = 1/2[111]$ line tension to become negative, leading to smooth loops, as observed. The beginnings of the tendency towards hexagonal shape are evident, though the prediction is fairly close to circular. For the $\boldsymbol{b} = [100]$ case at 500 ℃ however, negative line tension regions appear, and the methods of the previous section lead to a more squared-off shape, in agreement with the observations. These temperatures are in the $1/2\langle 111\rangle - \langle 100\rangle$ crossover regime, where the elastic anisotropy begins to dominate. As demonstrated in Ref.[6], the energy of $\langle 100\rangle$-type loops falls relative to that of $1/2\langle 111\rangle$-types as the anisotropy increases with temperature, in contrast with the isotropic elasticity approximation, where $1/2\langle 111\rangle$-types always have lower energy by virtue of their smaller Burgers' vector. The results presented here unambiguously confirm this behaviour, and explain why sharp-cornered hexagonal loops are not often observed in Fe: when the anisotropy is sufficient to yield polygonal $1/2\langle 111\rangle$ loops, their formation will be energetically-unfavourable compared with the $\langle 100\rangle$-types. [22]

The theoretical predictions described above were obtained using an idealized model, which neglects several important features of crystal dislocations. Firstly, it is a continuum approximation, and hence cannot capture the discrete behaviour of the atoms involved in a dislocation loop. This could explain the slightly rounded corners of the square $\langle 100\rangle$ loops in Fig.3C. Whilst this could be a microscope artefact, due to the complex strain field around a corner, it is also probable that the line-tension approximation breaks down in its immediate vicinity. Also, the continuum approximation allows the tangent angle ψ to take a continuous spectrum of values, whereas in a real crystal ψ is discrete, depending on the local crystallography. Secondly, $\langle 100\rangle$ loops smaller than about 20nm appear to have a more circular form. Again, this is probably due to the failure of the line-tension approximation at short distances, where non-local and inelastic contributions to the dislocation energy cannot be neglected. The finer-grained approach of MD simulations is required to address these issues, and provide a more complete theoretical understanding of the loop structure. However, the model accurately captures the mesoscale behaviour of the prismatic loops, and

demonstrates the importance of including anisotropic elastic effects when modelling iron (and ferritic steels) at temperatures above 400 ℃ .

The authors acknowledge helpful discussions with S.L. Dudarev, M. Kirk, M. L. Jenkins and M. Hernandez-Mayoral. This work was supported by the UK Engineering and Physical Sciences Research Council and by EURATOM. The views and opinions expressed herein do not necessarily reflect those of the European Commission.

---

[1] D. Bacon, R. Bullough, and J. Willis, Philos. Mag. **22**, 31 (1970).

[2] M. Gilbert, Z. Yao, M. Kirk, M. Jenkins, and S. Dudarev, Accpeted J. Nucl. Mat. **XX**, XXXX (2009).

[3] A. Morton, Philos. Mag. **A52**, 99 (1985).

[4] M. Jenkins, Z. Yao, M. Hernández-Mayoral, and M. Kirk, accepted J. Nucl. Mater. **XX**, XXX (2009).

[5] M. Puigvi, Y. Osetsky, and A. Serra, Philos. Mag. **83**, 857 (2003).

[6] S. L. Dudarev, R. Bullough, and P. Derlet, Phys. Rev. Lett. **100**, 135503 (2008).

[7] Y. Chou and G. Sha, Scripta Met. **7**, 201 (1973).

[8] S. Fitzgerald and S. Dudarev, Proc. R. Soc. London A **464**, 2549 (2008).

[9] G. deWit and J. S. Koehler, Phys. Rev. **116**, 1113 (1959).

[10] A. Head, M. Loretto, and P. Humble, Phys. Status Solidi **20**, 505 (1967).

[11] A. Head, M. Loretto, and P. Humble, Phys. Status Solidi **20**, 521 (1967).

[12] A. Head, Phys. Status Solidi **19**, 185 (1967).

[13] D. Barnett and D. Yaney, Scripta Met. **20**, 787 (1986).

[14] L. Wang and J. Lothe, Philos. Mag. **A71**, 359 (1995).

[15] G. Wulff, Z. Kristallogr. **34**, 449 (1901).

[16] Q. Jian, J. Maclennan, and N. Clark, Phys. Rev. E **56**, 1833 (1996).

[17] G. Schoeck and H. Kirchner, J. Phys. F: Met. Phys. **8**, L43 (1978).

[18] S. Gavazza and D. Barnett, J. Mech. Phys. Solids **24**, 397 (1975).

[19] D. Bacon, D. Barnett, and R. Scattergood, Prog. Mater. Sci. **23**, 51 (1980).

[20] D. Dever, J. Appl. Phys. **43**, 3293 (1972).

[21] I. Gelfand and S. Fomin, *Calculus of Variations* (Prentice-Hall, Eaglewood Cliffs, NJ, 1963).

[22] The observation of hexagonal $1/2\langle 111\rangle$ loops in β-brass is possible because the high anisotropy regime occurs at a lower temperature than in α-iron. This allows the persistence of metastable $1/2\langle 111\rangle$ loops which are not present in iron, where the higher temperature allows for thermally-activated transitions to the most stable ($\langle 100\rangle$) state.